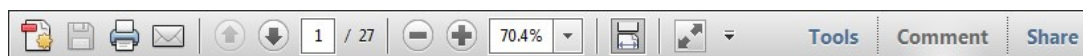
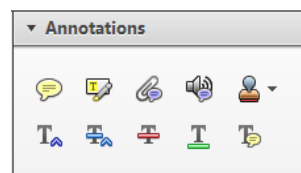


Once you have Acrobat Reader open on your computer, click on the [Comment](#) tab at the right of the toolbar:



This will open up a panel down the right side of the document. The majority of tools you will use for annotating your proof will be in the [Annotations](#) section, pictured opposite. We've picked out some of these tools below:



1. [Replace \(Ins\)](#) Tool – for replacing text.

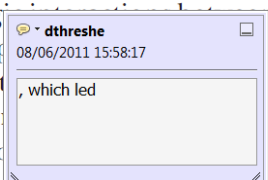


Strikes a line through text and opens up a text box where replacement text can be entered.

How to use it

- Highlight a word or sentence.
- Click on the [Replace \(Ins\)](#) icon in the Annotations section.
- Type the replacement text into the blue box that appears.

standard framework for the analysis of microeconomic behavior. Nevertheless, it also led to the development of strategic form games. The number of competitors in the market is that the strategic form game is a main component. At the micro level, are exogenous variables and important works on entry by firms (M henceforth) we open the 'black b



2. [Strikethrough \(Del\)](#) Tool – for deleting text.



Strikes a red line through text that is to be deleted.

How to use it

- Highlight a word or sentence.
- Click on the [Strikethrough \(Del\)](#) icon in the Annotations section.

there is no room for extra profits as mark-ups are zero and the number of firms (set) values are not determined by Blanchard and ~~Kiyotaki~~ (1987), perfect competition in general equilibrium of aggregate demand and supply in the classical framework assuming monopoly between an exogenous number of firms

3. [Add note to text](#) Tool – for highlighting a section to be changed to bold or italic.



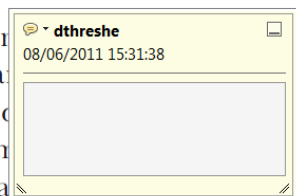
Highlights text in yellow and opens up a text box where comments can be entered.

How to use it

- Highlight the relevant section of text.
- Click on the [Add note to text](#) icon in the Annotations section.
- Type instruction on what should be changed regarding the text into the yellow box that appears.

dynamic responses of mark-ups consistent with the **VAR** evidence

sation by Markov. The standard framework for the analysis of microeconomic behavior. The number of competitors in the market is that the strategic form game is a main component. At the micro level, are exogenous variables and important works on entry by firms (M henceforth) we open the 'black b



4. [Add sticky note](#) Tool – for making notes at specific points in the text.

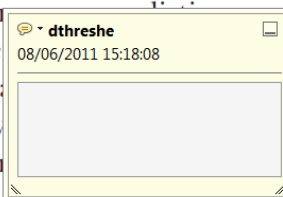


Marks a point in the proof where a comment needs to be highlighted.

How to use it

- Click on the [Add sticky note](#) icon in the Annotations section.
- Click at the point in the proof where the comment should be inserted.
- Type the comment into the yellow box that appears.

standard and supply shocks. Most of the standard framework for the analysis of microeconomic behavior. The number of competitors in the market is that the strategic form game is a main component. At the micro level, are exogenous variables and important works on entry by firms (M henceforth) we open the 'black b



5. **Attach File** Tool – for inserting large amounts of text or replacement figures.

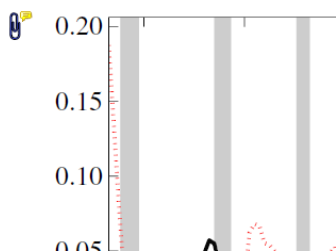


Inserts an icon linking to the attached file in the appropriate place in the text.

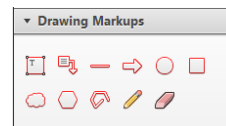
How to use it

- Click on the **Attach File** icon in the Annotations section.
- Click on the proof to where you'd like the attached file to be linked.
- Select the file to be attached from your computer or network.
- Select the colour and type of icon that will appear in the proof. Click OK.

END

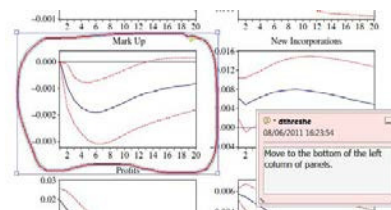


6. **Drawing Markups** Tools – for drawing shapes, lines and freeform annotations on proofs and commenting on these marks. Allows shapes, lines and freeform annotations to be drawn on proofs and for comment to be made on these marks.



How to use it

- Click on one of the shapes in the Drawing Markups section.
- Click on the proof at the relevant point and draw the selected shape with the cursor.
- To add a comment to the drawn shape, move the cursor over the shape until an arrowhead appears.
- Double click on the shape and type any text in the red box that appears.



A Novel Microsensor for Measuring Angular Distribution of Radiative Intensity

2 Thomas E. Murphy^{1*}, Stuart Pilorz², Leslie Prufert-Bebout¹ and Brad Bebout¹

¹NASA Ames Research Center, Moffett Field, CA

²SETI Institute, Mountain View, CA

Received 27 January 2015, accepted 7 March 2015, DOI: 10.1111/php.12452

ABSTRACT

This article presents the design, construction and characterization of a novel type of light probe for measuring the angular radiance distribution of light fields. The differential acceptance angle (DAA) probe can resolve the directionality of a light field in environments with steep light gradients, such as microbial mats, without the need to remove, reorient, and reinsert the probe, a clear advantage over prior techniques. The probe consists of an inner irradiance sensor inside a concentric, moveable light-absorbing sheath. The radiative intensity in a specific zenith direction can be calculated by comparing the irradiance onto the sensor at different acceptance angles. We used this probe to measure the angular radiance distribution of two sample light fields, and observed good agreement with a conventional radiance probe. The DAA probe will aid researchers in understanding light transfer physics in dense microbial communities and expedite validation of numerical radiative transfer models for these environments.

INTRODUCTION

The radiative intensity, or radiance, is the fundamental unit of radiative transfer (1,2). It is defined as the photon (or energy) flux in a specified zenith and azimuth direction per unit solid angle, per unit area normal to the incident beam (1,3,4). This quantity is dependent on wavelength of light, location and time. At any point in space within an illuminated medium, the radiance field describes the spectral radiance traveling through that point in all directions. This field is also known as the angular radiance distribution.

Measurement of the angular radiance distribution is an essential task in a wide variety of scientific fields. In atmospheric air quality monitoring, measurement of the directional radiance field is used as a standard way of estimating particulate size and refractive index (5), as these parameters largely control the scattering phase function of particles (6,7). In oceanography, measurement of the angular radiance distribution as a function of depth is essential to understanding and model scattering and absorption properties of different waters (8). In turn, these properties can be used to calculate attenuation rates of photosynthetically active radiation, which is essential for global primary

productivity modeling (9–12). The same light transfer physics apply to engineered ponds and photobioreactors for commercial algae cultivation (13–15) and attached algal biofilms for commercial chemical production or water decontamination (16–18).

Many devices have been developed to measure the angular radiance distribution in the underwater environment. One technique is to automatically sweep a radiance probe with a small acceptance angle through all directions (19). An alternative technique is to use a fisheye lens that maps light intensity from discretized directions onto a pixel array (20–22). Another commonly used oceanographic instrument is the Bio-Optical Profiling System (BOPS) (23), which enables inference of the downward- and upward-directed fluxes at various depths.

Primary productivity often occurs in environments with light gradients over the scale of millimeters, making the aforementioned underwater radiance instruments unfeasible. This is the case for photosynthetic communities such as soils (24), mosses and lichens (25), algal thalli (26), leaves of higher plants (27) and phototrophic biofilms for wastewater remediation and biofuel production (16). Research on the physiological responses of these systems to varying light regimes requires careful measurement of spatial light gradients on the μm -scale.

Of particular interest are microbial mats, light-driven ecosystems in which local metabolic rates are directly controlled by light availability (28–33). Microbial mats are vertically stratified ecosystems, typically one to several centimeters thick, containing a consortium of photosynthetic and nonphotosynthetic microorganisms in discrete sublayers, each having different spectral absorption and scattering properties (34). Understanding light transport within mats is important in that light-driven metabolic reactions within primitive biomats are thought to have transformed the early Earth's biosphere (35–38). It is also hypothesized that early life on exoplanets would likely exist in the form of photosynthetic biomats (39,40), and that spectral signatures of life-containing exoplanets could be influenced ultimately by the light transport within these ecosystems.

The dense nature of microbial mats compared to open ocean waters presents experimental and modeling challenges. From an experimental perspective, steep light gradients necessitate the use of microsensors for adequate depth resolution. From a modeling perspective, the microorganism size and spacing are such that the reliability of classical radiative transfer in treating scattering is called into question. In general, when the size of and spacing between scattering particles is large compared to the wavelength of light, classical radiative transfer theory can be used to

*Corresponding author e-mail: thomasemurphy@utexas.edu (Thomas E. Murphy)
© 2015 The American Society of Photobiology

calculate the light field, using relatively straightforward methods (1,2). However, when the particle size and spacing are comparable to the wavelength of light, particles exist in each other's near fields, and Maxwell's electromagnetic wave equations must be solved to calculate the light field, which is less straightforward (41,42). Siegel and Howell (1) provide a map of situations in which classical radiative transfer can and cannot be used to treat scattering phenomena, depending on the size and spacing of the scatterers. Indeed, mats straddle the border between these two regions. Evaluating the accuracy of different classical and non-classical radiative transfer models requires the development of microsenors that can quickly measure the angular radiance distribution at different depths in mats.

Researchers have predominantly used three types of light probes for quantifying light fields in mats: irradiance probes, scalar irradiance probes, and field radiance probes. The irradiance microprobe measures the cosine-weighted downwelling (or upwelling) irradiance, and consists of a light diffusing flat slab in front of an optical fiber (43). The irradiance microprobe is useful in measuring the irradiance reflectance (ratio of upwelling to downwelling irradiance), which is a useful parameter in calculating layer-by-layer energy balances. Second, the scalar irradiance microprobe measures the directionally integrated intensity from all directions (44,45). The scalar irradiance is the driving parameter for photosynthetic activity (10,20), and therefore these probes have gained popularity in microbial mat research (28,29,32,33,46). However, neither the irradiance nor the scalar irradiance microprobe can resolve the directionality of the radiance field, and therefore their utility in evaluating the accuracy of different mat radiative transfer models is limited.

The field radiance probe is unique and complementary, in that it can resolve the directional dependence of light intensity. The field radiance probe presented in Ref. (47) consisted of a bare optical fiber that had been tapered to a 20–30 μm tip and had a field of view with a half acceptance angle of about 30° . In two different studies, the angular radiance distribution in mats was measured by inserting a field radiance probe into mats at different angles (28,48). In these experiments, changing the direction of the probe required removing it and reinserting it at a specific angle. Thus, acquisition of an entire data set required significant time and labor, and placing the probe at the same location upon each reinsertion was tedious and difficult.

To expedite measurement of the angular radiance distribution in environments with steep light gradients, we designed and constructed a novel type of light probe. Our probe consists of an inner irradiance sensor (cosine collector) inside of a moveable concentric light-absorbing outer sheath. The distance between the irradiance sensor and the opening of the outer sheath controls the acceptance angle of the probe. The azimuthally averaged intensity is calculated by comparing the difference in irradiance onto the sensor as the acceptance angle is varied. This principle was first proposed for the underwater environment in (49) and (50), although the equipment they used was large and impractical for use in mats. Our “differential acceptance angle” (DAA) probe has been designed for assessing horizontally stratified fields, although it may be oriented in different directions. This will be the topic of future work. In this paper, we describe the construction of the DAA probe and then characterize its performance in comparison with a traditional field radiance probe.

MATERIALS AND METHODS

Theory. Figure 1 shows the principle of operation of the differential acceptance angle (DAA) radiance probe, which measures the azimuthally averaged radiative intensity as a function of the zenith angle. As the working model for the sensor, we consider a cylindrical tube sheath of circular radius a . Inside the sheath is an irradiance sensor at a distance d from the aperture. The walls of the tube sheath above the sensor are uniformly black. The acceptance angle of this tube is defined as

$$\theta_a = \tan^{-1}\left(\frac{a}{d}\right). \quad (1)$$

Any pencil beam of light having an angle of less than θ_a with respect to the center axis of the tube will strike the sensor, and any beam with a larger angle will strike the side of the tube and be absorbed before reaching the sensor. We also define μ_a as the cosine of the acceptance angle.

Given an arbitrary light field at the aperture, the flux seen by the sensor with acceptance angle θ_a is measured as

$$G(\mu_a) = \int_0^{2\pi} \int_{\mu_a}^1 I(\mu, \phi) R(\mu) d\mu d\phi, \quad (2)$$

where $R(\mu)$ is the angle-dependent response function of the sensor to light incident with a cosine of μ with respect to the normal. In practice, for the design presented here, the deviation of this response function from unity is largely due to a drop of epoxy sealant. We have verified that the sensor response is azimuthally uniform.

For a horizontally stratified field in which the sensor is oriented vertically, so that the light field depends only on θ , the angle with respect to the normal line of the sensor, the fundamental theorem of calculus allows us to write,

$$I(\mu) R(\mu) = \frac{1}{2\pi} \frac{dG(\mu)}{d\mu}, \quad (3)$$

where $2\pi d\mu$ carries units of steradians. In the case where $R(\mu)$ is equal to one, it is trivial to solve Eq. (3) for the radiance field, $I(\mu)$. More generally, we use our sensor to estimate the average radiance over a small range of θ :

$$\bar{I}(\mu_a) = \frac{\int_0^{2\pi} \int_{\mu_1}^{\mu_2} I(\mu, \phi) R(\mu) d\mu d\phi}{\int_0^{2\pi} \int_{\mu_1}^{\mu_2} R(\mu) d\mu d\phi}. \quad (4)$$

Equation (4) can be reduced to:

$$\bar{I}(\mu_a) = \frac{G\left(\mu_a - \frac{\delta\mu}{2}\right) - G\left(\mu_a + \frac{\delta\mu}{2}\right)}{2\pi R(\mu) d\mu}, \quad (5)$$

where $\bar{I}(\mu)$ is the average response between μ_1 and μ_2 . Equation (5) states that the average intensity between zenith angles 1 and 2 is a result of the irradiance incident onto the sensor at acceptance angle 2, but not at acceptance angle 1. Much of the sensor calibration involves estimating the response function $R(\mu)$. Equation (5) still applies in the case when the field is not azimuthally symmetric, as when the sensor is tilted with respect to vertical in a horizontally stratified field, or when there are significant inhomogeneities in the field.

Concerns over diffraction at the aperture. In order to qualify the diffraction effects within our device, we use the classical treatment of a plane wave normally incident on a plane punctured by a circular aperture. The circular aperture is identified with the circular opening of our device. In general, a plane wave incident from any angle is transmitted as a central beam surrounded by fringes. We expect diffraction to cause inaccuracies in our probe if a significant portion of an incident beam within a given acceptance angle is diffracted toward the absorbing wall before

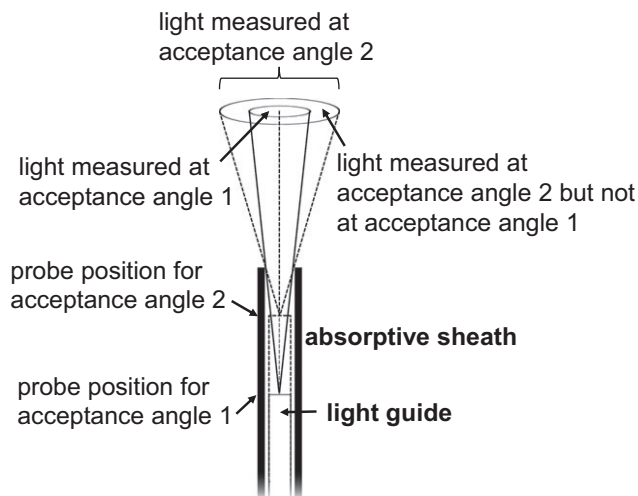


Figure 1. Operating principle of the differential acceptance angle (DAA) radiance probe.

reaching the detector, or if a significant portion of a beam outside the acceptance angle is diffracted toward the detector.

To address the concern of diffraction inaccuracies, consider a plane wave traveling into the sensor, normal to the opening of the sensor. The diffracted field of the incident normal wave is azimuthally symmetrical, and the intensity decreases with increasing angle with respect to the axis of the sensor, θ . This field can be described by solving the Fraunhofer equation (51). For light of wavelength λ , and an aperture of radius a , the intensity as a function of angle is expressed by the Airy function (51):

$$I(\theta) = I_0 \left(\frac{2J_1(x \sin \theta)}{x \sin \theta} \right)^2, \quad (6)$$

where $x = 2\pi a/\lambda$ and J_1 is a Bessel function of the first kind. Thus, the radius of the aperture relative to the wavelength of the light completely determines the behavior of $I(\theta)$. The intensity has a maximum at $\theta = 0$ and decreases with increasing θ . The oscillating zeros of the Airy function describe the locations of the diffraction fringes.

The first three zeros of the Airy function are at $x \sin \theta = 3.83, 7.02$, and 10.17 . For our purposes, we note that 93.8% of the power is contained within the third fringe at $x \sin \theta$ equal to 10.17 . The diffraction is most pronounced at long wavelengths, so we consider the behavior for a fiber optic device with a radius a equal to 0.5 mm and NIR light at a wavelength λ equal to 1 μm . For these numbers, we derive that the angular width of the cone containing 93.8% of the power would have a cone angle of 5×10^{-7} degrees. In our experimental setup, the uncertainty in acceptance angle caused by uncertainty in sensor depth and aperture diameter is on the order of a degree, much larger than the uncertainty caused by diffraction from the aperture. Therefore, we generally expect diffraction to be a relatively unimportant effect.

Probe construction. Figure 2 shows the components of the probe. The interior light guide (Thorlabs, part no. BFH48-600) consisted of a silica core (a), hard polymer cladding (b), and Tefzel™ coating (c) with diameters of 600, 630, and 1040 μm , respectively. Prior to assembling the probe, one end of the light guide was coupled to an SMA adapter and the other end was scissor cut. The cladding and coating within 5 mm of the scissor cut end were burned away with a flame. The exposed fiber core was made flat by grinding it against a spinning steel wheel covered in diamond paste. The light guide was then positioned inside a stainless steel tube (d) with an inner diameter of 1070 μm (McMaster-Carr, part no. 2180T13) such that the fiber core end was 1 mm from the opening of the steel tube. The space between the end of the light guide and the opening of the steel tube was filled with magnesium oxide (MgO) powder (e) (J.T. Baker, cas no. 1309-48-4), which served as a scattering material for desensitizing the response of the light guide to the direction of incoming light. A small drop of 5 Minute™ epoxy was placed onto the end of the tube to contain the MgO powder. The same epoxy was also used to fix the light guide to the inside of the steel tube. The steel tube containing the light guide and the MgO powder comprised the

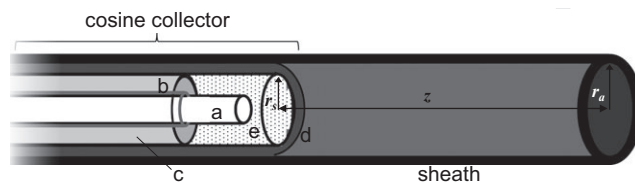


Figure 2. Schematic of the DAA probe components, showing the (a) glass core, (b) hard polymer cladding, and (c) Tefzel™ coating of the light guide inside a (d) steel tube filled with (e) magnesium oxide powder. Parts (a)–(e) comprise the cosine collector, which was placed inside the Acktar Metal Velvet™ light-absorbing sheath.

cosine collector. The sheath surrounding the cosine collector consisted of an Acktar Metal Velvet™ adhesive foil sheet that had been rolled into a cylinder with a length of 50 mm and a radius r_a of 1.0 mm. The Metal Velvet™ material was selected based on its low hemispherical reflectivity of 0.01 in the visible spectral range of 400–700 nm. To control the acceptance angle, the cosine collector was translated within the sheath, using a micromanipulator with a resolution of 10 μm (World Precision Instruments Inc., model M3301R).

Probe characterization. First, the photoelectrical response of the inner cosine collector was measured as a function of incident beam angle. Then, the DAA probe was used to measure the angular radiance distribution of two sample light fields. For each field, a conventional Gershun tube radiance probe was used for benchmarking. The Gershun tube probe was made by placing the cosine collector at a fixed depth of 10 mm within the 2 mm diameter sheath for an acceptance half angle of 5.7° . For both the Gershun tube probe and the DAA probe, the interior of the sheath was approximated as perfectly nonreflecting, which is justified as the hemispherical reflectance of the interior material was reported by the manufacturer as less than 1% in the visible range.

Radiometric measurement. For all experiments, the SMA end of the light guide of the cosine collector was connected to a spectrometer (Ocean Optics, USB4000), which was connected to a computer via USB. The Ocean Optics SpectraSuite™ software package was used to record the signal from the spectrometer at a wavelength near the emission maximum of the light source under investigation. It should be noted that the signal from the spectrometer was measured in “counts,” as a radiometric calibration to convert to Watts or photons per second was not performed. For this reason, henceforth, radiative intensities measured in a given experiment are normalized to the maximum radiative intensity measured in that experiment.

Cosine collector characterization. The cosine collector without the sheath was evaluated for directional sensitivity. For this, the cosine collector was mounted onto a protractor (General Mfg. Co. Inc., part no. 48) and exposed to a collimated light beam provided by an LED power supply (Oriel, model 66088) and passed through a collimating lens (Oriel, 77799). The angle of the incident beam was varied between 0° and 90° by controlling the protractor angle.

DAA probe characterization. The DAA probe was used to measure the angular radiance distribution underneath two different light sources. Light source 1 was a 75 Watt incandescent light bulb (Philips) equipped with a 14 cm diameter reflector (Underwriters Laboratories, AH-2131). The position of measurement for light source 1 was 7 cm underneath the center of the bulb, and the intensity was measured at 680 nm. Light source 2 consisted of an LED array equipped with a 10 cm diameter diffuser. The array consisted of LEDs of 16 different peak wavelengths, although for this experiment only the signal at 632 nm was recorded. The location of measurement was 3 cm below the center of the diffuser. A micromanipulator was used to vary the distance between the sheath opening and the cosine collector and therefore the acceptance angle of the probe. The intensity as a function of zenith angle was calculated according to Eq. (5). Three sets of measurements were performed to quantify uncertainty.

As a benchmark, the Gershun tube probe was used to measure the angular radiance distribution for the same two light fields. For this, the Gershun tube probe was mounted to a protractor, which was mounted to a ring stand. The zenith angle was controlled by the protractor angle, and the azimuthal angle was controlled by rotating the entire ring stand. The intensity I in direction (θ, ϕ) was calculated as,

$$I(\theta, \phi) = \frac{G(\theta, \phi)}{\Omega_p}, \quad (7)$$

where $G(\theta, \phi)$ is the irradiance onto the sensor and Ω_p is the acceptance solid angle of the probe, equal to 0.031 sr. For light source 1, the intensity at each zenith angle was measured at three different azimuthal angles. Due to the greater azimuthal heterogeneity of light source 2, the intensity at each zenith angle was measured at seven different azimuthal angles. The average intensity and standard deviation were calculated at each zenith angle. The results were then compared to those obtained using the DAA probe.

RESULTS

Cosine collector characterization

Figure 3 shows the response of the cosine collector as a function of incident collimated beam angle. All responses were normalized by the maximum response, and error bars represent the standard deviation between measurements from three separate trials. The cosine function is also shown, which represents an ideal response. The figure indicates that, at incidence angles less than 65°, the cosine collector had a response that was less than ideal by an average of 4% (as percentage of maximum response). At incidence angles between 70° and 90°, the cosine collector had a response that was on average 8% (of maximum response) greater than the ideal response.

The difference between the cosine collector response and the ideal response was likely due to the curvature of the epoxy cap that was used to contain the magnesium oxide powder in the sensor. At beam incidence angles less than 60°, the curved cap caused local increases in the beam incidence angle on the non-beam-facing half of the cap, thereby increasing its reflectance relative to a perfectly flat cap. At incidence angles greater than 60°, however, the protrusion of the cap into the axial dimension of the sensor increased the projected area of the cap as seen by the beam. In future designs, this issue can be mitigated by manipulating the surface tension of the epoxy used for the cap, which will in turn control its curvature. The response function $R(\theta)$ is presented in Table 1.

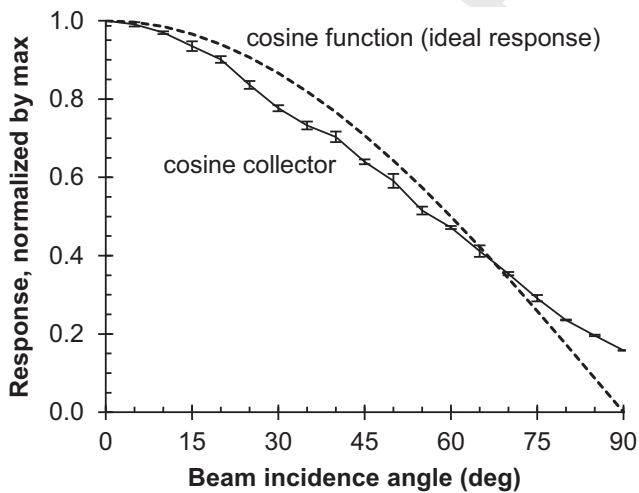


Figure 3. Response of the bare cosine collector as a function of incident beam angle. The response at each incident angle is normalized by the maximum response. The cosine function is also shown, which represents an ideal response.

DAA probe characterization

The angular radiance distribution underneath each test light source was measured using both the DAA probe and a conventional Gershun tube radiance probe. For the DAA probe, Fig. 4 shows a sample data set of the signal from the light guide as a function of acceptance angle underneath light source 1. The signal did not increase appreciably as the acceptance angle increased from 45° to 90°, which is indicative of the low intensities in directions that were not in view of the lamp.

The radiative intensity as a function of the zenith angle as measured by the DAA probe was recovered from the raw data using Eq. (5). This intensity is shown alongside the intensity as measured by the Gershun tube probe in Fig. 5. Error bars for the DAA probe data were calculated as standard deviation between three replicate trials. Error bars for the Gershun tube data were calculated as the standard deviation between three azimuthal angles for light source 1 and seven azimuthal angles for light source 2. For light source 1, the maximum intensity was observed at a zenith angle of about 25° from vertical as a result of the focusing effect of the lamp's reflector. The angular radiance distribution as measured by the two probes are generally in good agreement, with the exception of zenith angles between 35° and 55°, where the intensity as measured by the DAA probe was on average 17% (as percent of maximum intensity) higher than the benchmark intensity. Outside this region, average discrepancy between the DAA probe and the benchmark was 3%.

Figure 5b shows the angular radiance distribution for light source 2. In contrast with light source 1, light source 2 featured a broad plateau of intensity at zenith angles between 0° and 45°, which was caused by the diffuser in front of the LED array. The region of maximum disagreement between the two probes occurred at zenith angles between 20° and 45°. In this region, the DAA probe overestimated the benchmark intensity by an average of 8% (as percent of maximum intensity), whereas the average discrepancy was only 2% outside this zenith region.

DISCUSSION

The differential acceptance angle (DAA) light probe was used to measure the angular radiance distribution of two sample light fields with good accuracy compared to a conventional Gershun tube radiance probe. The greatest discrepancy in intensity occurred at moderate zenith angles (35–55° for light source 1 and 20–45° for light source 2). In these regions, the intensity as measured by the DAA probe was on average 13% higher (as percentage of maximum intensity) than the intensity as measured by the Gershun tube probe. Outside this zenith angle region, the

Table 1. Response function $R(\theta)$ of the cosine collector.

Beam angle, θ (deg)	Response function, $R(\theta)$
5	0.99
15	0.97
25	0.92
35	0.89
45	0.90
55	0.90
65	0.97
75	1.13
85	2.25

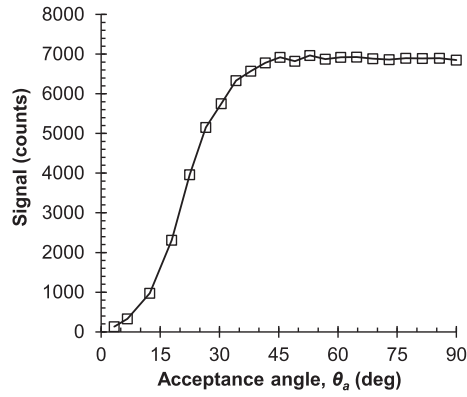


Figure 4. Sample data for the DAA probe under the light source 1.

agreement between the two probes was within 3%. The discrepancy between the probes at moderate zenith angles is attributed to the curvature and large diameter of the cosine collector relative to the sheath diameter. The calculation of the acceptance angle (Eq. 1) utilizes the assumption that the cosine collector is a point acceptor at the center of the sheath at a specific depth. However, in practice, the curvature of the epoxy cap causes the cosine collector to protrude from its nominal depth within the sheath, such that its actual depth is somewhat ambiguously defined. Moreover, the cosine collector in this study had a diameter of about 1 mm, compared to a sheath diameter of 2 mm. Therefore, the acceptance angle was actually slightly larger than that calculated by Eq. (1). However, the curvature of the epoxy cap made it difficult to calculate the acceptance angle exactly because beams striking the cap at grazing angles were less likely to be transmitted through the light guide. For these reasons, future designs will focus on incorporating a cosine collector with a much smaller diameter than that of the sheath. The drawback of a smaller cosine collector is a decreased signal to noise ratio.

Despite these shortcomings specific to this particular design iteration, the DAA probe significantly expedites the measurement of the angular radiance distribution relative to previous techniques. In the context of microbial mats, conventional techniques for measuring the angular radiance distribution require repeatedly reinserting a field radiance probe into the mat at different angles (28,48). This process is time and labor-intensive. Moreover, it is difficult to place the field radiance probe at the same location upon each reinsertion. On the other hand, the design of the DAA

probe enables acquisition of the same data while only requiring the probe to be inserted once, vertically, into the mat.

It should be noted that azimuthal dependence of the radiative intensity cannot be detected with the DAA probe. However, most previous studies on radiative transfer in mats have made use of a normally incident, collimated light source, in which case an azimuthal dependence of radiative intensity is not expected (28,48). For such applications, the DAA probe exhibits larger signal to noise ratios than conventional field radiance probes because the solid angle of measurement covers the entire azimuthal range simultaneously.

Some challenges remain for using DAA probes in dense microbial mats. For one, the outer diameter of the probe presented in this study was 2.2 mm, which was chosen due to ease of construction. However, it is desirable to traverse the depth of a microbial mat without disturbing its structure, which requires a needle tip with a diameter on the order of 10–100 μm . Future designs will focus on this scale constraint. Furthermore, the fluid inside the sheath in the current study was air, which is nonabsorbing and nonscattering at this length scale. When using a DAA probe in a participating medium, it will be important to keep the medium inside the sheath as nonparticipating as possible, so as not to distort the signal by scattering and absorbing photons traveling from the sheath opening to the cosine collector. To accomplish this, the sheath can be designed with a diameter small enough such that the surrounding viscous fluid cannot enter, or a “filler” fluid can be preloaded into the sheath and pushed out into the surrounding fluid as the acceptance angle is increased.

CONCLUSIONS

This article presented a novel type of light probe for measuring the angular radiance distribution of light fields. This differential acceptance angle (DAA) probe consists of an interior irradiance sensor and a concentric light-absorbing sheath. The acceptance angle of the probe is controlled by varying the depth of the irradiance sensor within the sheath. A methodology was presented for recovering the angular distribution of radiative intensity from the function of irradiance onto the sensor as a function of acceptance angle. The DAA probe was used to measure the angular radiance distribution of two sample light fields. These radiance distributions were then compared to the distributions as measured by a conventional Gershun tube probe. Agreement was good

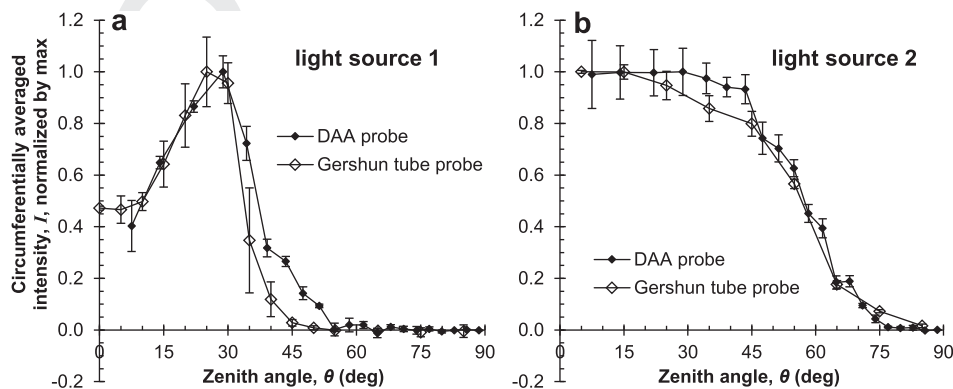


Figure 5. Angular radiance distribution under (a) light source 1, an incandescent bulb with a reflector, and (b) light source 2, an LED array behind a diffuser, as measured by the differential acceptance angle (DAA) probe as well as the Gershun tube radiance probe.

between the two probes, with an average discrepancy of 13% at moderate zenith angles between 20° and 55° and about 3% at zenith angles outside this range. It is expected that this type of light probe will aid researchers in understanding light transfer physics within photosynthetic communities with steep light gradients with an accuracy and speed significantly greater than previously achieved.

Acknowledgements—The authors gratefully acknowledge the financial support provided by the NASA Postdoctoral Program.

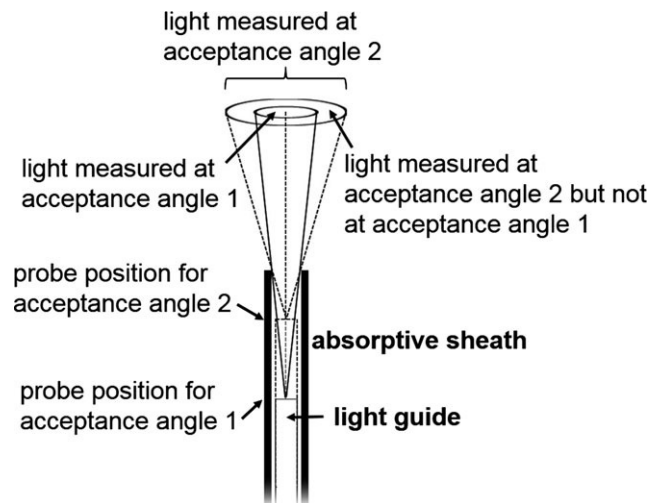
REFERENCES

- Siegel, R. and J. Howell (2002) *Thermal Radiation Heat Transfer*, 4th edn. Taylor & Francis, New York, NY.
- Modest, M. F. (2003) *Radiative Heat Transfer*. Academic Press, San Diego, CA.
- Lewis, M. R., J. Wei, R. Van Dommelen and K. J. Voss (2011) Quantitative estimation of the underwater radiance distribution. *J. Geophys. Res.* **116**, 1–14.
- Incropera, F., D. Dewitt, T. Bergman and A. Lavine (2007) *Fundamentals of Heat and Mass Transfer*, 6th edn. John Wiley & Sons, Hoboken, NJ.
- Boylan, J. W. and A. G. Russell (2006) PM and light extinction model performance metrics, goals, and criteria for three-dimensional air quality models. *Atmos. Environ.* **40**, 4946–4959.
- Hansen, J. E. and L. D. Travis (1974) Light scattering in planetary atmospheres. *Space Sci. Rev.* **16**, 527–610.
- Mishchenko, M. I., J. Hovenier and L. Travis (eds.) (1999) *Light Scattering by Nonspherical Particles*. Academic Press, New York, NY.
- Kirk, J. T. (1983) *Light and Photosynthesis in Aquatic Ecosystems*. Cambridge University Press, Cambridge.
- Smith, R. C. and W. H. Wilson (1972) Photon scalar irradiance. *Appl. Opt.* **11**, 934–938.
- Morel, A. (1991) Light and marine photosynthesis: A spectral model with geochemical and climatological implications. *Prog. Ocean.* **26**, 263–306.
- Heinermann, P. H., L. Johnson and M. A. Ali (1990) The underwater photic environment of a small arctic lake. *Arctic* **43**, 129–136.
- Kywalyangav, M., T. Platt and S. Sathyendranath (1992) Ocean primary production calculated by spectral and broad-band models. *Mar. Ecol. Prog. Ser.* **85**, 171–185.
- Cornet, J.-F. and C.-G. Dussap (2009) A simple and reliable formula for assessment of maximum volumetric productivities in photobioreactors. *Biotechnol. Prog.* **25**, 424–435.
- Berberoglu, H. and L. Pilon (2010) Maximizing the solar to H₂ energy conversion efficiency of outdoor photobioreactors using mixed cultures. *Int. J. Hydrogen Energ.* **35**, 500–510.
- Lee, E., J. Pruvost, X. He, R. Munipalli and L. Pilon (2014) Design tool and guidelines for outdoor photobioreactors. *Chem. Eng. Sci.* **106**, 18–29.
- Christenson, L. B. and R. C. Sims (2012) Rotating algal biofilm reactor and spool harvester for wastewater treatment with biofuels by-products. *Biotechnol. Bioeng.* **109**, 1674–1684.
- Murphy, T. E. and H. Berberoglu (2014) Flux balancing of light and nutrients in a biofilm photobioreactor for maximizing photosynthetic productivity. *Biotechnol. Prog.* **30**, 348–359.
- Schultze, L. K. P., M.-V. Simon, T. Li, D. Langenbach, B. Podola and M. Melkonian (2015) High light and carbon dioxide optimize surface productivity in a Twin-Layer biofilm photobioreactor. *Algal Res.* **8**, 37–44.
- Duntley, S. Q., R. J. Uhl, R. W. Austin, A. R. Boileau and J. E. Tyler (1955) An underwater photometer. *J. Opt. Soc. Am.* **45**, 904(A).
- Smith, R. C., R. W. Austin and J. E. Tyler (1970) An oceanographic radiance distribution camera system. *Appl. Opt.* **9**, 2015–2022.
- Voss, K. J. and A. Chapin (2005) Upwelling radiance distribution camera system, NURADS. *Opt. Express* **13**, 4250–4262.
- Wei, J., R. Van Dommelen, M. R. Lewis, S. McLean and K. J. Voss (2012) A new instrument for measuring the high dynamic range radiance distribution in near-surface sea water. *Opt. Express* **20**, 27024–27038.
- Smith, R. C., C. R. Booth and J. L. Star (1984) Oceanographic bio-optical profiling system. *Appl. Opt.* **23**, 2791–2797.
- Rajeev, L., U. N. da Rocha, N. Klitgord, E. G. Luning, J. Fortney, S. D. Axen, P. M. Shih, N. J. Bouskill, B. P. Bowen, C. A. Kerfeld, F. Garcia-Pichel, E. L. Brodie, T. R. Northen and A. Mukhopadhyay (2013) Dynamic cyanobacterial response to hydration and dehydration in a desert biological soil crust. *ISME J.* **7**, 2178–2191.
- Heber, U., N. G. Bukhov, V. A. Shuvalov, Y. Kobayashi and O. L. Lange (2001) Protection of the photosynthetic apparatus against damage by excessive illumination in homoiohydric leaves and poikilohydric mosses and lichens. *J. Exp. Bot.* **52**, 1999–2006.
- Binzer, T. and K. Sand-Jensen (2002) Production in aquatic macrophyte communities: A theoretical and empirical study of the influence of spatial light distribution. *Limnol. Oceanogr.* **47**, 1742–1750.
- Vogelmann, T. C. and L. Björn (1984) Measurement of light gradients and spectral regime in plant tissue with a fiber optic probe. *Physiol. Plant.* **60**, 361–368.
- Kühl, M., L. C. and B. B. Jørgensen (1994) Light penetration and light intensity in sandy marine sediments measured with irradiance and scalar irradiance fiber-optic microprobes. *Mar. Ecol. Prog. Ser.* **105**, 139–148.
- Oren, A., M. Kühl and U. Karsten (1995) An endoevaporitic microbial mat within a gypsum crust: Zonation of phototrophs, photopigments, and light penetration. *Mar. Ecol. Prog. Ser.* **128**, 151–159.
- Garcia-Pichel, F. and B. M. Bebout (1996) Penetration of ultraviolet radiation into shallow water sediments: High exposure for photosynthetic communities. *Mar. Ecol. Prog. Ser.* **131**, 257–262.
- Wiggli, M., A. Smallcombe and R. Bachofen (1999) Reflectance spectroscopy and laser confocal microscopy as tools in an ecophysiological study of microbial mats in an alpine bog pond. *J. Microbiol. Methods* **34**, 173–182.
- Hawes, I. and A.-M. J. Schwarz (2000) Absorption and utilization of irradiance by cyanobacterial mats in two ice-covered Antarctic lakes with contrasting light climates. *J. Phycol.* **37**, 5–15.
- Al-Najjar, M. A. A., D. de Beer, M. Kühl and L. Polerecky (2012) Light utilization efficiency in photosynthetic microbial mats. *Environ. Microbiol.* **14**, 982–992.
- Stal, L. and P. Caumette (eds.) (1994) *Microbial Mats*. Springer, Berlin.
- Hoehler, T. M., B. M. Bebout and D. J. Des Marais (2001) The role of microbial mats in the production of reduced gases on the early Earth. *Nature* **412**, 324–327.
- Bebout, B. M., T. M. Hoehler, B. Thamdrup, D. Albert, S. P. Carpenter, M. Hogan, K. Turk and D. J. Des Marais (2004) Methane production by microbial mats under low sulphate concentrations. *Geobiology* **2**, 87–96.
- de Wit, R., F. P. van den Ende and H. van Gernerden (1995) Mathematical simulation of the interactions among cyanobacteria, purple sulfur bacteria and chemotrophic sulfur bacteria in microbial mat communities. *FEMS Microbiol. Lett.* **17**, 117–136.
- Decker, K. L. M., C. S. Potter, B. M. Bebout, D. J. Des Marais, S. Carpenter, M. Discipulo, T. M. Hoehler, S. R. Miller, B. Thamdrup, K. A. Turk and P. T. Visscher (2005) Mathematical simulation of the diel O₂, S, and C biogeochemistry of a hypersaline microbial mat. *FEMS Microbiol. Ecol.* **52**, 377–395.
- Kiang, N. Y., J. Siefert, ????. Govindjee and R. E. Blankenship (2007) Spectral signatures of photosynthesis. I. Review of Earth organisms. *Astrobiology* **7**, 222–251.
- Sanromá, E., E. Pallé, M. N. Parenteau, N. Y. Kiang, A. M. Gutiérrez-Navarro, R. López and P. Montañés-Rodríguez (2014) Characterizing the purple Earth: Modeling the globally integrated spectral variability of the Archean Earth. *Astrophys. J.* **780**, 1–11.
- Mishchenko, M. I. (2008) Multiple scattering, radiative transfer, and weak localization in discrete random media: Unified microphysical approach. *Rev. Geophys.* **46**, 1–33.
- Tishkovets, V. P. and E. V. Petrova (2013) Light scattering by densely packed systems of particles: Near-field effects. In *Light Scattering Reviews 7: Radiative Transfer and Optical Properties of Atmosphere and Underlying Surface* (Edited by A. A. Kokhanovsky), pp. 3–36. Springer Praxis Books, Berlin.

43. Lassen, C. and B. B. Jørgensen (1994) A fiber-optic irradiance microsensor (cosine collector): Application for in situ measurements of absorption coefficients in sediments and microbial mats. *FEMS Microbiol. Ecol.* **15**, 321–336.
44. Lassen, C., H. Ploug and B. B. Jørgensen (1992) A fibre-optic scalar irradiance microsensor: Application for spectral light measurements in sediments. *FEMS Microbiol. Ecol.* **86**, 247–254.
45. Garcia-Pichel, F. (1995) A scalar irradiance fiber-optic microprobe for the measurement of ultraviolet radiation at high spatial resolution. *Photochem. Photobiol.* **61**, 248–254.
46. Kühl, M. and B. B. Jørgensen (1992) Spectral light measurements in microbenthic phototrophic communities with a fiber-optic microprobe coupled to a sensitive diode array detector. *Limnol. Oceanogr.* **37**, 1813–1823.
47. Jørgensen, B. B. and D. J. Des Marais (1986) A simple fiber-optic microprobe for high resolution light measurements: Application in marine sediment. *Limnol. Oceanogr.* **31**, 1376–1383.
48. Jørgensen, B. B. and D. J. Des Marais (1988) Optical properties of benthic photosynthetic communities: Fiber-optic studies of cyanobacterial mats. *Limnol. Oceanogr.* **33**, 99–113.
49. Johnson, N. G. and G. Liljequist (1938) On the angular distributions of submarine daylight and on the total submarine illumination. *Sven. Hydrogr. - Biol. Komm. Skr. Ny. Ser. Hydrogr.* **14**, 1–15.
50. Pettersson, H. (1938) Measurements of the angular distribution of submarine light. *Rapp. Cons. Explor. Mer.* **108**, 7–12.
51. Born, M. and E. Wolf (1999) *Principles of Optics: Electromagnetic Theory of Propagation, Interference, and Diffraction of Light*, 7th edn. Cambridge University Press, Cambridge.

Graphical Abstract

The contents of this page will be used as part of the graphical abstract of html only. It will not be published as part of main article.



Measurement of the directional dependence of radiative intensity is essential for understanding light transport in microbial mats, plant leaves, soils and phototrophic biofilms. Previously, measuring the directional intensity in these environments required inserting a field radiance probe with a small acceptance angle into a tissue at multiple angles, which required significant time and labor. This paper presents a novel differential acceptance angle (DAA) light probe, which can measure the directional intensity in light fields from a single location without reorienting the probe. We discuss the construction of the DAA probe and its performance compared to a conventional **4** field radiance probe.

Author Query Form

Journal: PHP
Article: 12452

















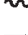



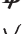





























Dear Author,

During the copy-editing of your paper, the following queries arose. Please respond to these by marking up your proofs with the necessary changes/additions. Please write your answers on the query sheet if there is insufficient space on the page proofs. Please write clearly and follow the conventions shown on the attached corrections sheet. If returning the proof by fax do not write too close to the paper's edge. Please remember that illegible mark-ups may delay publication. Many thanks for your assistance.

Query reference	Query	Remarks
1	AUTHOR: This article has been lightly edited for grammar, style, and usage. Please compare it with your original document and make changes on these pages. Please limit your corrections to substantive changes that affect meaning. If no change is required in response to a question, please write "OK as set" in the margin.	
2	AUTHOR: Please confirm that given names (red) and surnames/family names (green) have been identified correctly.	
3	AUTHOR: Please check that authors and their affiliations are correct.	
4	AUTHOR: Please confirm that graphical abstract is fine for online publication.	
5	AUTHOR: Please check equations to ensure that they have been entered correctly.	
6	AUTHOR: Please provide the given names/initials for the author Govindjee for reference [39].	

Proof Correction Marks

Please correct and return your proofs using the proof correction marks below. For a more detailed look at using these marks please reference the most recent edition of The Chicago Manual of Style and visit them on the Web at: <http://www.chicagomanualofstyle.org/home.html>

<i>Instruction to typesetter</i>	<i>Textual mark</i>	<i>Marginal mark</i>
Leave unchanged	... under matter to remain	
Insert in text the matter indicated in the margin		 followed by new matter
Delete	 through single character, rule or underline or  through all characters to be deleted	
Substitute character or substitute part of one or more word(s)	 through letter or  through characters	new character  or new characters 
Change to italics	 under matter to be changed	
Change to capitals	 under matter to be changed	
Change to small capitals	 under matter to be changed	
Change to bold type	 under matter to be changed	
Change to bold italic	 under matter to be changed	
Change to lower case		
Insert superscript		 under character e.g. 
Insert subscript		 over character e.g. 
Insert full stop		
Insert comma		
Insert single quotation marks	 	 
Insert double quotation marks	 	 
Insert hyphen		
Start new paragraph		
Transpose		
Close up	linking  characters	
Insert or substitute space between characters or words		
Reduce space between characters or words	